ARMY RESEARCH LABORATORY

An Assessment of Potential Nonlinear Circuit Models for the Characterization of Resonant Tunneling Diodes

Dwight L. Woolard, Felix A. Buot, David L. Rhodes,
Xiaojia Lu and Barry S. Perlman

ARL-TR-1119 July 1996

DISCLAIMER NOTICE

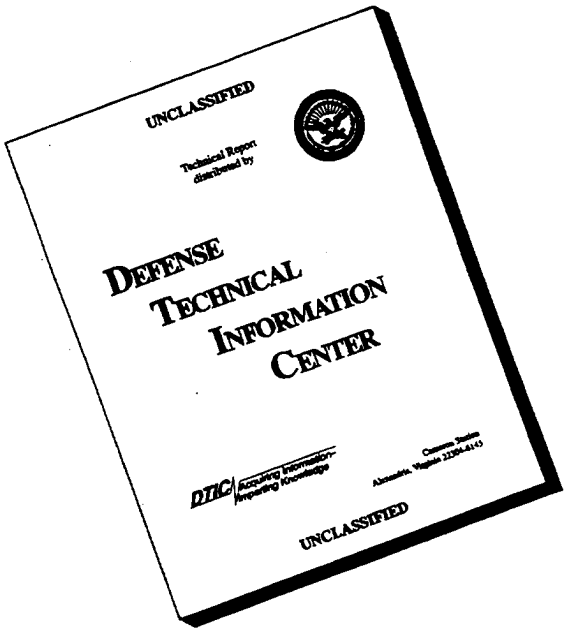

THIS DOCUMENT IS BEST QUALITY AVAILABLE. THE COPY FURNISHED TO DTIC CONTAINED A SIGNIFICANT NUMBER OF PAGES WHICH DO NOT REPRODUCE LEGIBLY.

NOTICES

Disclaimers

The findings in this report are not to be construed as an official Department of the Army position, unless so designated by other authorized documents.

The citation of trade names and names of manufacturers in this report is not to be construed as official Government endorsement or approval of commercial products or services referenced herein.

REPORT DOCUMENTATION PAGE

Form Approved
OMB No. 0704-0188

1. AGENCY USE ONLY *(Leave blank)*	2. REPORT DATE	3. REPORT TYPE AND DATES COVERED
	July 1996	Technical Report

4. TITLE AND SUBTITLE
An Assessment of Potential Nonlinear Circuit Models for the Characterization of Resonant Tunneling Diodes

5. FUNDING NUMBERS

6. AUTHOR(S)
Dwight L. Woolard, Felix A. Buot,* David L. Rhodes, Xiaojia Lu, Barry S. Perlman

7. PERFORMING ORGANIZATION NAME(S) AND ADDRESS(ES)
US Army Research Laboratory (ARL)
Physical Sciences Directorate
ATTN: AMSRL-PS-EA
Fort Monmouth, NJ 07703-5601

8. PERFORMING ORGANIZATION REPORT NUMBER
ARL-TR-1119

9. SPONSORING/MONITORING AGENCY NAME(S) AND ADDRESS(ES)

10. SPONSORING/MONITORING AGENCY REPORT NUMBER

11. SUPPLEMENTARY NOTES
*Felix A. Buot is with the Naval Research Laboratory, Washington, DC 20375-5320.

12a. DISTRIBUTION/AVAILABILITY STATEMENT
Approved for public release; distribution is unlimited.

12b. DISTRIBUTION CODE

13. ABSTRACT *(Maximum 200 words)*

The intrinsically fast process of resonant tunneling through double barrier heterostructures along with the existence of negative differential resistance in the current-voltage characteristic of these structures has led to their implementation as sources for high frequency electromagnetic energy. While sources based upon resonant tunneling diodes (RTD's) have produced frequency of oscillations up to 712 GHz, only microwatt levels of performance have been achieved above 100 GHz. Since stability criteria play a critical role in determining the deliverable power of any oscillator, a physically accurate equivalent-circuit model for the RTD is extremely important for optimizing the dynamics of the device-cavity package. This study identifies a distinctly new equivalent circuit model for characterizing the modes of oscillation in RTD-based sources. Specifically, in order to exhibit the fundamental self-oscillations and the overall I-V characteristics (plateau structure and hysteresis) observed experimentally, an accurate circuit model of the RTD must incorporate: (1) a quantum-well inductance which directly chokes the nonlinear conductance, and (2) a nonlinear access resistance, associated with the accumulation of charge in the injection region of the double barriers, with a nonlocal dependence on the bias across the double barrier structure.

14. SUBJECT TERMS
resonant tunneling, oscillations, bistable, high frequency electronics, equivalent circuit model

15. NUMBER OF PAGES
16

16. PRICE CODE

17. SECURITY CLASSIFICATION OF REPORT	18. SECURITY CLASSIFICATION OF THIS PAGE	19. SECURITY CLASSIFICATION OF ABSTRACT	20. LIMITATION OF ABSTRACT
Unclassified	Unclassified	Unclassified	UL

CONTENTS

		Page
I.	Introduction	1
II.	Circuit Model Characteristics	2
III.	Numerical Simulation Study	3
	A. Series-Inductance Model: Constant Parameters	3
	B. Parallel-Inductance Model: Constant Parameters	4
	C. Series-Inductance Model: Nonlinear R(V) Model	6
	D. Parallel-Inductance Model: Nonlinear R(V) Model	7
	E. Parallel-Inductance Model: Nonlinear R(V) and L(V) Models	8
IV.	Conclusion	9
	References	9
	Biographies	10

FIGURES

1.	Basic circuit configurations used in nonlinear oscillation study.	2
2.	Overall current-density versus applied bias derived from Wigner distribution simulation	2
3.	Overall current-density solutions for forward, backward and tri-stable state for condition of absolute stability (i.e., no self-oscillations)	4
4.	Current-voltage phase-space trajectory of a self-oscillating condition	5
5.	Overall current-density versus applied bias derived from series-inductance circuit model with constant parameters.	5
6.	Overall current-density versus applied bias derived from parallel-inductance circuit model with constant parameters.	5
7.	Current-density phase-space trajectories for forward and backward bias sweeps at an applied bias of 0.22 V	6
8.	Time evolution of the total current-density for the forward bias sweep at an applied bias of 0.22 V.	6
9.	Limit-cycle of the z-v space trajectory for the forward bias sweep at an applied bias of 0.22 V.	6
10.	Access resistance as a function of voltage across the intrinsic RTD structure	7
11.	Intersection curves of $I(V)$ characteristic and nonlinear loadline for a range of applied biases.	7
12.	Overall current-density versus applied bias derived from series-inductance circuit with nonlinear $R(V)$ model.	7
13.	Overall current-density versus applied bias derived from paralleled-inductance circuit with nonlinear $R(V)$ model.	8
14.	Time evolution of the total current-density for the forward bias sweep at an applied bias of 0.26 and 0.28 V with $L = 5.5 \times 10^{-21}$ Hcm^2.	8
15.	Overall current-density versus applied bias derived from parallel-inductance circuit with nonlinear $R(V)$ model and nonlinear $L(V)$ model.	8

An Assessment of Potential Nonlinear Circuit Models for the Characterization of Resonant Tunneling Diodes

Dwight L. Woolard, *Member, IEEE*, Felix A. Buot, *Member, IEEE*, David L. Rhodes, *Member, IEEE*, Xiaojia Lu, and Barry S. Perlman, *Fellow, IEEE*

***Abstract*—The intrinsically fast process of resonant tunneling through double barrier heterostructures along with the existence of negative differential resistance in the current-voltage characteristic of these structures has led to their implementation as sources for high frequency electromagnetic energy. While sources based upon resonant tunneling diodes (RTD's) have produced frequency of oscillations up to 712 GHz, only microwatt levels of performance has been achieved above 100 GHz. Since stability criteria play a critical role in determining the deliverable power of any oscillator, a physically accurate equivalent-circuit model for the RTD is extremely important for optimizing the dynamics of the device-cavity package. This study identifies a distinctly new equivalent circuit model for characterizing the modes of oscillation in RTD-based sources. Specifically, in order to exhibit the fundamental self-oscillations and the overall I-V characteristics (plateau structure and hysteresis) observed experimentally, an accurate circuit model of the RTD must incorporate; (i) a quantum-well inductance which *directly* chokes the nonlinear conductance and, (ii) a nonlinear access resistance, associated with the accumulation of charge in the injection region of the double barriers, with a *nonlocal* dependence on the bias across the double barrier structure.**

I. Introduction

APPLICATION of resonant tunneling diodes (RTD) to high-frequency/high-speed electronics is attractive due to the fundamental physical principles upon which they operate. The RTD, as was first demonstrated by Chang *et al.* [1], exhibits the purely quantum mechanical process of tunneling where electrons transverse the double-barrier structure via the quasibound energy state of the well. Since this tunneling occurs through the quantum-well state(s) which first becomes aligned and then passes by emitter states in the source [2] during a bias sweep, the RTD yields a negative differential resistance (NDR) current characteristic. Furthermore, since tunneling is an intrinsically fast process the RTD current can respond very rapidly to changes in applied bias. In fact, RTD's have been shown experimentally to have detection capabilities up to 2.5 THz [3] and have been implemented as oscillators up to 712 GHz [4]. Therefore, the remarkable fast-acting NDR of RTD's make them excellent devices for very high-frequency electronic applications.

RTD's have been extensively investigated as sources of terahertz (10^{12} Hz) electromagnetic energy. Unfortunately, RTD-based power sources have only demonstrated microwatt levels (i.e. <50 μW) of performance above 100 GHz [5]. Thus, RTD's have been outperformed in this frequency band by more traditional sources (e.g. IMPATT's, TUNNET's, etc.) and the power levels achieved are not sufficient for many practical applications [6]. The high frequency potential of RTD's has concentrated much effort toward the theoretical optimization of these structures using a number of material systems [7]. While quantum simulations [8]–[10] are necessary to derive the fundamental characteristics of isolated structures, equivalent circuit models are usually employed to determine the power and stability limitations of an RTD within an actual resonating cavity or circuit. To date, such estimations of RTD performance have been based upon linear oscillation theory and/or have utilized simple small-signal diode models [11]. Obviously, the results hinge upon the equivalent circuit model used in the analysis. Hence, efforts to optimize the power performance of RTD-based sources can be curtailed if the choice and/or approach to circuit modeling is not an accurate representation of the dynamics of the device-cavity package. Therefore, the identification of a equivalent circuit model which closely matches the physical dynamics is extremely important in the design and optimization of RTD oscillators.

A phenomenon which is commonly observed during the experimental probing of the NDR current-region of RTD's is the development of oscillations with bistable behavior. In some cases, these spurious oscillations can not be eliminated and interfere with the measurement of the negative conductance of the device [12]. While there has been some debate over whether these oscillations are a result of extrinsic (i.e. induced by external bias circuit) or intrinsic factors [13], [14], recent quantum mechanical simulations of a completely isolated structure indicate the RTD has an inherent ability to self-oscillate. These theoretical results [15] are free of the extrinsic influences always present during experimental measurements yet exhibit characteristics observed in actual measurements such as a plateau and a hysteresis effect. In fact, comparing the I-V results from these quantum-based simulations (i.e. see Fig. 2) to experimental measurements of a similar RTD structure (e.g. [5]) reveals a remarkable agreement in the

D. L. Woolard, D. L. Rhodes, X. Lu, and B. S. Perlman are with the U.S. Army Research Laboratory, PSD, Fort Monmouth, NJ 07703-5601 USA

F. A. Buot is with the Naval Research Laboratory, Washington, D.C. 20375-5320 USA.

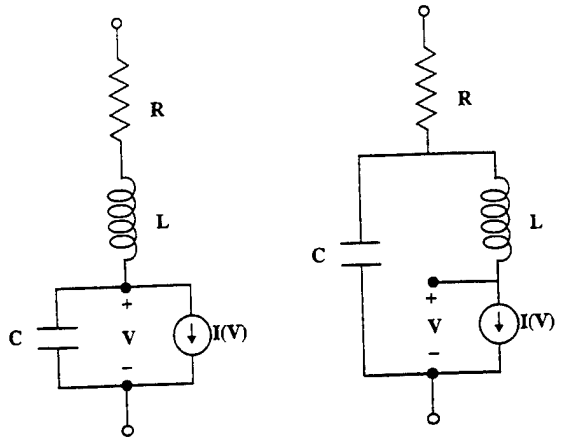

Fig. 1. Basic circuit configurations used in nonlinear oscillation study.

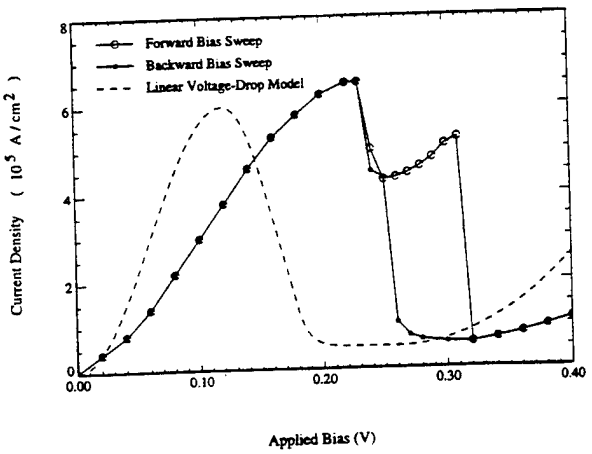

Fig. 2. Overall current-density versus applied bias derived from Wigner distribution simulation.

plateau and step-like features. Hence, these observations verify the presence of multiple electric storage effects in the *intrinsic* RTD structure. These self-oscillations are useful because they can be used as a guide to determining an accurate equivalent circuit model for the purely intrinsic RTD.

The observation of self-oscillations in RTD's is also important from another perspective. For example, previous limitations on the output power of RTD-based sources can be directly linked to the manner of their implementation. Traditionally, RTD's are implemented purely as a NDR element with one energy storage element (i.e. device capacitance). Using this design approach, oscillations must be generated by limit-cycles which exchange energy with resonating elements residing in the external bias circuit. This approach of extrinsically inducing oscillations will always encounter output power restrictions by external losses (e.g. contact resistance) and low frequency design constraints (i.e. suppression of bias oscillations). However, this theoretically-observed self-oscillation process [15], which occurs due to the separate charging-delay times of the emitter accumulation region and the quantum-well, provides evidence for a possible intrinsic approach to high-frequency power generation. Since these oscillations have frequencies extending up to 6 THz and their amplitudes are not limited by external constraints, there is much motivation for better understanding this intrinsic process. Hence, the identification of an accurate equivalent circuit model for the RTD is valuable for providing insight on ways to encourage the occurrence of this intrinsic phenomenon and for guiding methods to couple this intrinsically-generated power to output circuitry.

This paper presents a comprehensive evaluation of the circuit model configurations presently in use for approximating the behavior of RTD's and extends them to arrive at a new model. In the studies presented, the numerically-generated nonlinear results associated with a number of autonomous second-order circuits are compared to the self-oscillations and the average current-density characteristics observed in the quantum mechanical simulations for a specific case. This work identifies a specific circuit model configuration which has the potential for matching the current-density characteristics observed both experimentally and theoretically. Specifically, this work reveals two major requirements of the model before it can accurately reproduce the fundamental self-oscillations and the overall I-V characteristics (i.e. plateau structure and hysteresis). First, the RTD circuit model must incorporate a quantum-well inductance which directly chokes the nonlinear conductance element. Second, the model must include a nonlinear "access" resistance. This new resistance model, associated with the accumulation of charge in the adjacent injection (emitter) region, possesses a nonlocal dependence on the bias across the double barrier structure. The results from the numerical simulation study, presented in Section III, will confirm the need for *both* of these elements in the equivalent circuit model. Specifically, a nonlinear (i.e. with nonlocal voltage dependence) access resistance is required to match the known hysteresis behavior. Furthermore, the circuit model must also include a quantum-well inductance before it can produce the correct self-oscillations and current-plateau phenomena. Finally, this work will show that nonlinear effects associated with this inductive element are responsible for some of the finer features of the oscillations and bistable behavior. These results are important because this new model will allow for the accurate optimization of output power in RTD-based high-frequency sources in the future.

II. Circuit Model Characteristics

The theoretical identification of an accurate large-signal equivalent-circuit model for the resonant tunneling diode (RTD) is important from a number of perspectives. An accurate circuit model is important in oscillator design for: (i) maximizing the power-frequency product which includes the suppression of low-frequency (LF) oscillations in the bias circuitry [11], [16]; (ii) extracting individual component characteristics from experimental measurements [17]–[19];

and (iii) providing insight for structural changes to the RTD which will lead to an improved device-cavity system [6].

In selecting the basic RTD circuit-model configurations for our study, we will utilize its fundamental physical characteristics as a guide. The *intrinsic* RTD is known to possess the following general characteristics: (i) a low-frequency I-V characteristic with a NDC region which arises from tunneling through quantum states near the resonant-state-energy of the double barrier structure; (ii) a capacitance due to the negative charges in the accumulated emitter and well imaging of the positive charge in the depleted collector; (iii) an access resistance associated with the highly doped bulk regions on either side of the double barrier structure; and (iv) a self-inductance which models the intrinsic delay in the tunneling current with respect to the barrier-well-barrier voltage [15], [20]. The basic circuit configurations selected for this nonlinear study are given in Fig. 1(a) and (b). Since every fundamental-mode oscillator requires at least two energy-storage elements [21], these two autonomous second-order nonlinear circuits represent the simplest forms which simultaneously satisfy all the characteristics itemized in (i) through (iv). The *series-inductance* (i.e. inductance is in series with device capacitance) model given in Fig. 1(a) was originally proposed by Gering *et al.* [22] to explain an experimentally observed resonance matching a series-inductance model. The *parallel-inductance* (i.e. inductance in parallel with device capacitance) model given in Fig. 1(b) is identical in circuit-form with the one proposed by Brown *et al.* [20].

The presentation which follows will compare the nonlinear large-signal behavior of each circuit to self-consistent quantum mechanical simulations of a specific RTD structure. In this study, each circuit is evaluated for its ability to match self-consistent Wigner-distribution-based simulations of a specific RTD geometry previously presented by Jensen and Buot [23]. This RTD is a GaAs-AlGaAs based structure with 30 Å barriers and a 50 Å well. The AlGaAs potential barriers are 0.3 eV and the device temperature is 77 K. The entire simulation region, including 2×10^{18} cm^3 doped buffer regions, is 550 Å. In this study, dissipation effects were included through both internal device scattering and open boundary conditions. Note, the very short simulation "box" employed does not influence the results since "free-flowing" (as opposed to traditional ohmic) boundary conditions were enforced [24], [25]. Time-dependent solutions for the response of this RTD structure yield the overall current-voltage (I-V) characteristic displayed in Fig. 2. For the forward sweep, current oscillations were observed within the voltage region $V = 0.24$ to $V = 0.32$. For the backward sweep, current oscillations were observed only over the small region $V = 0.24$ to $V = 0.25$. Also, given in Fig. 2 is a plot of the I-V curve when the entire applied voltage is assumed to drop linearly across the quantum barrier-well region. For this linear voltage-drop model all the results were static [15].

Note, the theoretical I-V curves in Fig. 2 display peak current-densities of approximately 6×10^5 A/cm^{-2} which are considerably greater than that typically reported for RTD's of comparable dimensions in this material system. However, it should be noted that conventional GaAs-AlGaAs RTD structures, which typically possess peak densities of less than 1×10^5 A/cm^{-2}, almost always employ undoped spacer layers (i.e. between buffer and barrier regions) and usually utilize limited doping levels in the emitter region [12]. This type of design is chosen for practical experimental devices to insure undoped barrier/well regions and to improve device contacts. Since the peak current density of an RTD is highly dependent on the electron density that resides at the emitter-barrier interface [5], these relatively higher values of current-density obtained for the structure under consideration (i.e. with highly doped emitter and no spacer layer) should be expected.

III. Numerical Simulation Study

In this section, a numerical simulation study is used to assess the accuracy of circuit models presently in use for predicting the high-frequency performance of RTD's. Here, a van der Pol based method [26] is used to solve for the nonlinear oscillations associated with each circuit under consideration. This work will show that previous models lack essential elements necessary for predicting the self-oscillations observed experimentally during measurements of the current-voltage characteristics [27] and predicted theoretically by quantum mechanical simulations [15].

A. Series-Inductance Model: Constant Parameters

The first equivalent circuit model considered is the series-inductance model, as given by Fig. 1(a), with constant values of energy storage elements (i.e. L and C) and constant access resistance R. Assuming that the series-inductance circuit is biased by a dc voltage source V_S, application of standard circuit relations readily yield the autonomous second-order nonlinear equation,

$$\frac{d^2v}{dt^2} + \eta(v, V_{\rm dc})\frac{dv}{dt} + \omega^2(v, V_{\rm dc})v = 0 \qquad (1)$$

where

$$\eta(v, V_{\rm dc}) = (LG(v, V_{\rm dc}) + RC)/(LC)$$
$$\omega^2(v, V_{\rm dc}) = (Rg(v, V_{\rm dc}) + 1)/(LC).$$

Equation (1) results from a transformation into the dc current-voltage frame of reference where the total voltage across the nonlinear element is $V(t) = v(t) + V_{\rm dc}$ and $V_{\rm dc}$ is the oscillation-free voltage in the circuit. Hence, (1) describes the evolution of v which is the transient component of voltage. This transformation explains the dc voltage dependence of the parameters, $g(v, V_{\rm dc}) = (I(v + V_{\rm dc}) - I(V_{\rm dc}))/v$ which can be defined as the *nonlinear* conductance, since in this frame the transient current density is $i = I(v + V_{\rm dc}) - I(V_{\rm dc}) = g(v, V_{\rm dc})v$, and $G(v, V_{\rm dc}) = G(V) = dI/dV$ which is just the slope of $I(V)$ at $V = v + V_{\rm dc}$ or the normal definition of the *linearized* conductance. This transformation allows solution of the nonlinear dc biasing separately from the time-dependent oscillation problem, although dynamic biasing effects are still inherently included.

After a modified Newton's method [28] was used to solve the biasing problem, a numerical version of the van der Pol algorithm [29] was employed to solve for the unstable (or

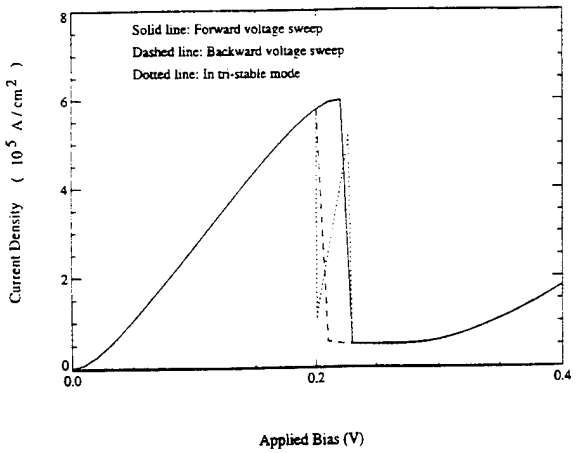

Fig. 3. Overall current-density solutions for forward, backward and tri-stable state for condition of absolute stability (i.e. no self-oscillations).

decaying) states of (1). This van der Pol-based algorithm is simply *two successive* numerical integrations performed on the system which results when (1) is written as two first order equations [26]. Specifically, introduction of the substitution variable $z = dv/dt = \dot{v}$ and using $\dot{z} = z \cdot (dz/dv)$ leads to the trajectory equation

$$\frac{dz}{dv} = -\eta(v, V_{\rm dc}) - \omega(v, V_{\rm dc})\left(\frac{v}{z}\right). \qquad (2)$$

In analogy with the method of isoclines or the phase-portrait technique [21], (2) is numerically integrated to generate a phase-space trajectory for z as a function of v. Solution curves for v as a function of time are then obtained by approximate integration of $z = dv/dt$.

For the initial circuit simulations of this case study, parameter values were estimated from previous quantum mechanical calculations. The nonlinear conductance $I(V)$ is defined from the linear voltage-drop model result in Fig. 2. The constant value for $R = 1.63 \times 10^{-7}\ \Omega\ \text{cm}^2$ was approximated from the shift in the *peak* of the I-V characteristic given in Fig. 2. The constant value of $C = 2.3 \times 10^{-7}$ F/cm^2 was obtained by calculating the total displaced charge as a function of the bias voltage and taking the average over the NDR region. The value of $L = 1.48 \times 10^{-21}$ H cm^2 was estimated by matching a linear oscillation analysis to the current-oscillations observed during the physical simulations. For a detailed discussion of the reasoning for these initial parameter choices refer to [15].

The first step of the analysis is the determination of $V_{\rm dc}$ which is obtained from the solution of $I(V) + (V - V_S)/R = 0$ where V_S is the applied bias. The important point to note is that for some values of V_S there are multiple solutions for the $V_{\rm dc}$-intercept. For example, consider the complete dc mapping which results from all intercept points as given in Fig. 3. Clearly, a hysteresis is present in this *oscillation-free* current-voltage characteristic $I_D(V_S)$ where: (i) the *forward* voltage sweep solution is associated with the low-V_S intercept point; (ii) the *backward* voltage-sweep solution is associated with the high-V_S intercept point; and (iii) the *tri-stable* solution is associated from the midpoint intercept.

The van der Pol algorithm was then applied to both the forward and backward sweeps to study the general stability of the series-inductance circuit model. The introduction of noise-vectors (impulses) and the subsequent generation of the z-v trajectories showed *decaying* solutions for all $V_{\rm dc}$ intercepts both within and outside the NDR (i.e. region where $G(v, V_{\rm dc}) < 0$). The same procedure was applied to the tri-stable $V_{\rm dc}$ intercepts and in all cases transients were observed which either converged to the forward-sweep or the negative-sweep $V_{\rm dc}$ intercepts appropriate for the applied bias under consideration. A variational study was also performed to determine if values of L and C could be found which led to oscillations. Studies over a wide range (i.e. ten times larger and smaller) of the base values $C_0 = 2.3 \times 10^{-7}$ F/cm^2 and $L_0 = 1.48 \times 10^{-21}$ H cm^2 yielded the same stable results. These results agree with a previous *linear* analysis which indicated that the series-inductance model was incapable of yielding the self-oscillations observed in the physical simulations with these estimated circuit parameters [15].

In an additional variational study of the access resistance R, oscillations were found to exist for values $R \leq 0.5 \times 10^{-7}\ \Omega\,\text{cm}^2$. Fig. 4 shows the phase-space trajectory of the main-lead current density for $R = 0.5 \times 10^{-7}\ \Omega\,\text{cm}^2$ and $L = L_0 = 1.48 \times 10^{-21}$ H cm^2 at an applied bias of $V_S = 0.179$ V. The period of this oscillation, which is 0.15 ps, matches one of the self-oscillations of the quantum simulations; however, it occurs at a *much lower* applied bias. Fig. 5 compares the average forward-sweep current versus bias for the three cases $L = L_0/5L_0$ and $5L_0$ with $R = 0.5 \times 10^{-7}\ \Omega\,\text{cm}^2$. For the oscillating cases, there is a development of a current-plateau for increasing values of L and a similar result (not shown) can be obtained for variations in C. For clarity, we have not shown the backward-sweep results which exhibits a hysteresis similar in extent to that seen in Fig. 3. These general results agree with previous studies of circuits with the series-inductance form [30], [31]. The *main point* to note is while one can achieve self-oscillations and a hysteresis effect with the *constant-parameter* series-inductance model by properly choosing L (or C) this can only be done by significantly reducing the estimated value of access resistance R. Since this reduction of R leads a large backward shift in the overall $I_D(V_S)$ characteristic, an overall match to the physics-based simulations is not possible.

B. Parallel-Inductance Model: Constant Parameters

The next circuit model considered is the parallel-inductance circuit model with constant parameters as given in Fig. 1(b). For the investigations of this model, the initial values employed for R, L and C will be the same as those defined in the last section. The dynamics of the parallel-inductance circuit are described by the nonlinear equation

$$\frac{d^2v}{dt^2} + \eta(v, V_{\rm dc})\frac{dv}{dt} + \zeta(v, V_{\rm dc})\left(\frac{dv}{dt}\right)^2 + \omega^2(v, V_{\rm dc})v = 0 \quad (3)$$

where

$$\eta(v, V_{\rm dc}) = (LG(v, V_{\rm dc}) + RC)/(RCLG(v, V_{\rm dc}))$$
$$\zeta(v, V_{\rm dc}) = (G'(v, V_{\rm dc}))/(G(v, V_{\rm dc}))$$
$$\omega^2(v, V_{\rm dc}) = (1 + Rg(v, V_{\rm dc}))/(RCLG(v, V_{\rm dc})).$$

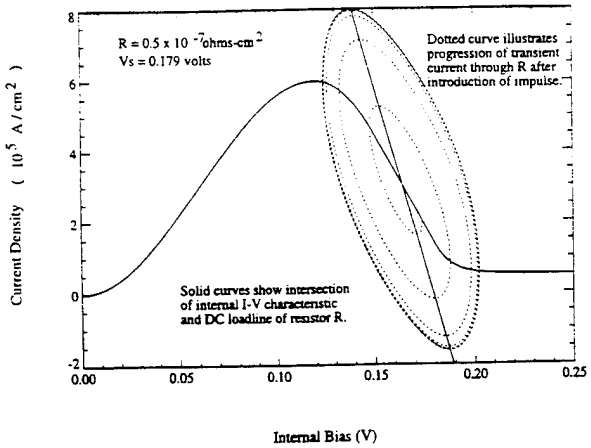

Fig. 4. Current-voltage phase-space trajectory of a self-oscillating condition

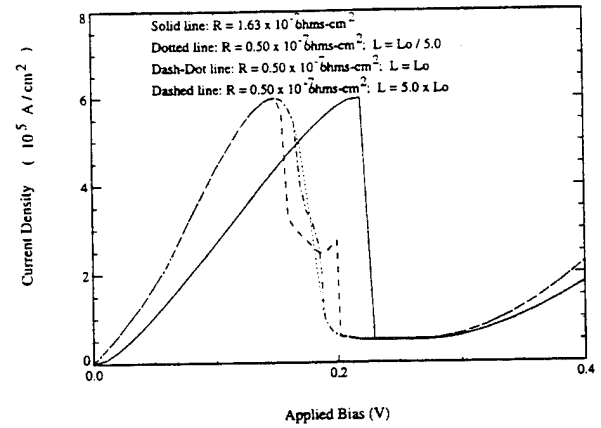

Fig. 5. Overall current-density versus applied bias derived from series-inductance circuit model with constant parameters.

Here, as before, $g(v, V_{\rm dc})$ is the *nonlinear* conductance and $G(v, V_{\rm dc})$ is the *linear* conductance. Since the dc circuit for this model is the same as that for the series-inductance model, the $V_{\rm dc}$ reference is defined by the same loadline intercepts as in the previous section. Also, note the emergence of the new parameter $\zeta(v, V_{\rm dc})$ containing the relation $G'(v, V_{\rm dc}) = G'(V) = dG/dV$ which is just the derivative of the linear conductance. Unlike the defining equation for the previous model, the coefficients for (9) all contain $G(v, V_{\rm dc})$ in their denominators; and hence, possess the potential to become singular. Later, this will be shown to lead to "jumps" in the phase-space trajectories.

The numerical algorithm was employed to investigate the stability of the parallel-inductance model for forward and backward bias sweeps. After determining the appropriate $V_{\rm dc}$-intercepts, the z-v space trajectory is then obtained by integration of

$$\frac{\partial z}{\partial v} = -\eta(v, V_{\rm dc}) - \zeta(v, V_{\rm dc})z - \omega^2(v, V_{\rm dc})\left(\frac{v}{z}\right) \qquad (4)$$

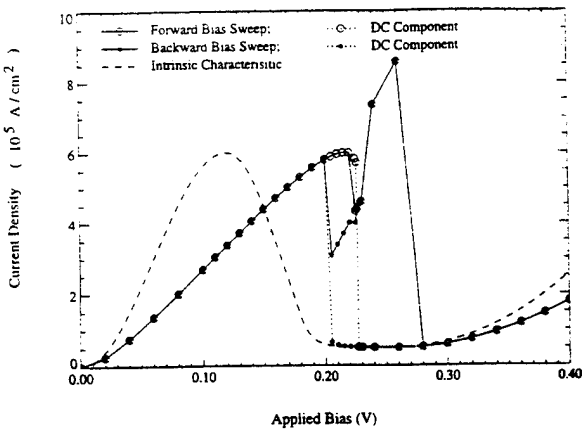

Fig. 6. Overall current-density versus applied bias derived from parallel-inductance circuit model with constant parameters.

and a time mapping is then achieved from $z = dv/dt$. Fig. 6 gives the overall current-density results for the estimated circuit parameters $R = 1.63 \times 10^{-7}\ \Omega\,\mathrm{cm}^2$, $C = 2.3 \times 10^{-7}\ \mathrm{F/cm}^2$, and $L = 1.48 \times 10^{-21}\ \mathrm{H\,cm}^2$. Note, the dc current components are also included for reference. In the applied bias range $(0.20, 0.23)$ the characteristic is found to display a distinct hysteresis with oscillations in both the forward and backward sweeps within the NDR. The origin of this hysteresis can be understood by referring to Fig. 7 which shows the phase-space trajectories for forward and backward bias sweeps at $V_S = 0.22$ V. While the final limit-cycles of the two trajectories are equivalent, the dc bias points for the forward and backward differ by a significant value. Thus, the overall (or total) current-density is a function of sweep direction. Another feature of note is the very rapid (but finite) changes in the current-density at the phase-space turning points. Fig. 8 gives the time domain representation of the forward-sweep trajectory from Fig. 7. As shown, these *jumps* in current-density correspond to instances where dv/dt is discontinuous. These *allowable* discontinuities in dv/dt arise from the intersection of the trajectory with the singular points defined by $G(v, V_{\rm dc}) = 0$ (recall this drives the coefficients in (9) to infinity). This phenomenon can be understood by referring to Fig. 9 which shows the final z-v space limit-cycle for the forward-sweep trajectory from Figs. 7 and 8. As the value of v approaches the point where $G(v, V_{\rm dc}) = 0$, the z ordinate is seen to approach infinity. However, a limit analysis of (9) as $G \to 0$ reveals that it degenerates to the first-order quadratic equation

$$(z)^2 + \left(\frac{1}{G'(v_J, V_{\rm dc})}\right)z + \left(\frac{Rg(v_j, V_{\rm dc}) + 1}{RCLG(v_j, V_{\rm dc})}\right) = 0 \qquad (5)$$

where $z = dv/dt$ and v_J is the jump value. Hence, as the z-v space trajectory makes its clockwise cycle and these singularities are encountered a jump occurs at the turning points. Here, the jump is from $z = \infty$ to the appropriate root of (5). In the numerical algorithm, all that is required is to estimate the location of the v-space turning point(s) and to integrate to a sufficiently large value of z to ensure the accuracy of the v and t mapping.

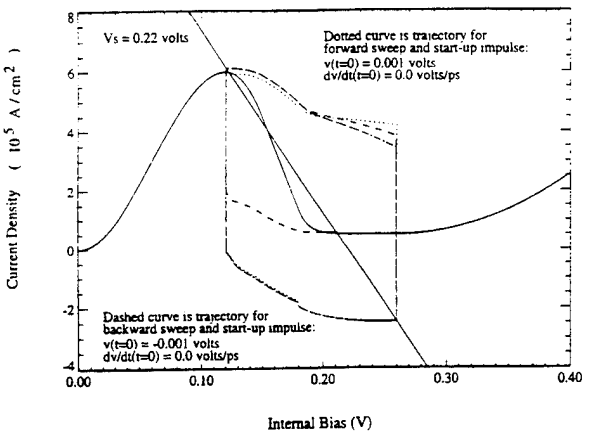

Fig. 7. Current-density phase-space trajectories for forward and backward bias sweeps at an applied bias of 0.22 V.

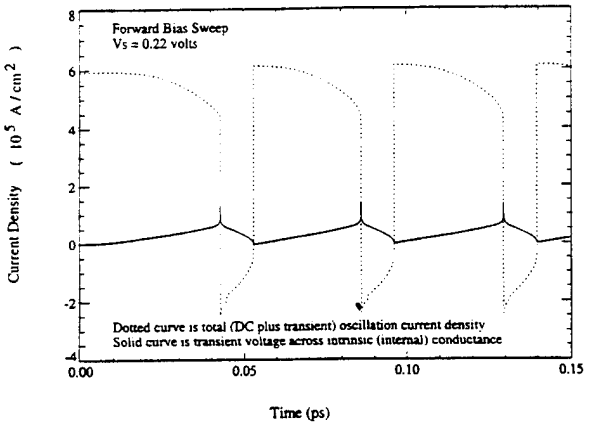

Fig. 8. Time evolution of the total current-density for the forward bias sweep at an applied bias of 0.22 V. Here, the internal conductance bias (scaled by a factor of ten is volts) is also plotted for reference.

Returning to a discussion of Fig. 6, the hysteresis collapses at $V_S \approx 0.23$ V; however, a plateau remains out to $V_S = 0.27$ V. This plateau is the result of an oscillation about an attractor in z-v space which occurs at a point near the low-voltage singularity. The oscillations of this plateau region are of a very high frequency (period $\ll 0.01$ ps) and of very small amplitude ($v \ll 0.01 \times 10^5$ A/cm^2). Thus, these current-density characteristics would *appear* as static if they were derived from simulations in a total reference frame or from actual measurements.

Simulations were also performed to determine how variations in L and/or C would influence the overall results. While these studies indicate that the hysteresis and plateau structure can be significantly altered by changes to these terms, the major discrepancies between the results of Fig. 6 and the physical-simulation results of Fig. 2 could not be resolved. Limitations of the parallel-inductance model with constant parameters: (i) a restricted region of hysteresis; (ii) oscillations present in the backward sweep; and (iii) incorrect amplitude and/or frequency of forward sweep self-oscillations.

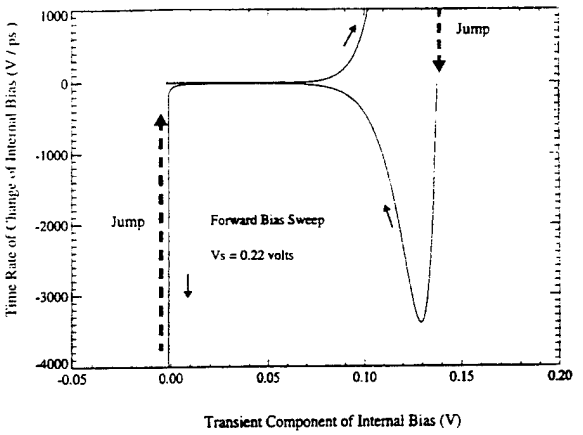

Fig. 9. Limit-cycle of the z-v space trajectory for the forward bias sweep at an applied bias of 0.22 V. This limit-cycle exhibits jumps at the turning points which correspond to the peak and valley of the nonlinear $I(V)$ characteristic.

Therefore, the constant-parameter parallel-inductance model is not suitable for describing the dynamics of the specific RTD under consideration.

The results of the last two sections have shown that neither of the basic circuit configurations *with constant parameters* is sufficient to describe the observed self-oscillations. While one should expect the presence of nonlinearities in the storage elements (i.e. C and L), the previous results suggest that the constant R is a barrier to achieving the correct hysteresis in the overall current-density characteristic. The value of the constant R, used up to this point, was estimated from the shift in the RTD's I-V characteristic when self-consistency effects are included. This approach is accurate only if the true access resistance is independent of bias. Since the backward sweep current-density given in Fig. 2 is almost (i.e. except for the small bias region $(0.24, 0.25)$) free of oscillations the voltage dependency of R can be easily estimated. A point by point estimation of the shift in the current-density can be used to determine the effective resistance as a function voltage across the barrier structure. The character of this voltage-dependent resistance $R(V)$ is given approximately by the piece-wise curve shown in Fig. 10. The influence of $R(V)$ on the previous circuit models will be considered in the sections which follow.

C. Series-Inductance Model: Nonlinear $R(V)$ Model

The transient response of the series-inductance model with nonlinear access resistance $R(V)$ and constant storage elements is described by the nonlinear equation

$$\frac{d^2v}{dt^2} + \eta(v, V_{\rm dc})\frac{dv}{dt} + \omega^2(v, V_{\rm dc})v = 0 \qquad (6)$$

where the coefficients are the same as in (1) with $R(V)$ substituted for R. Here, as before, $V_{\rm dc}$ is the reference frame which is found *now* by solving the dc loadline equation with the nonlinear $R(V)$. Fig. 11 displays a number of the loadline intercepts for (15) where $R(V)$ is defined from the characteristic given in Fig. 10. This nonlinear access resistance causes the resultant loadlines to sag downward in the NDR region increasing the range of V_S values over which multiple

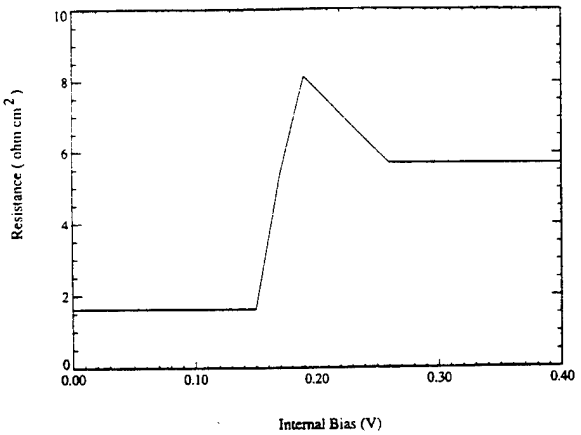

Fig. 10. Access resistance as a function of voltage across the intrinsic RTD structure.

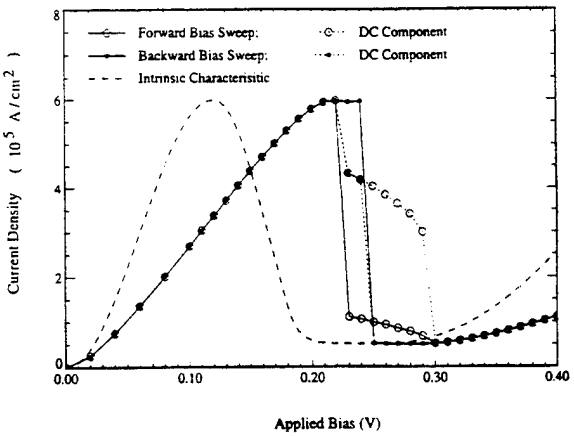

Fig. 12. Overall current-density versus applied bias derived from series-inductance circuit with nonlinear $R(V)$ model.

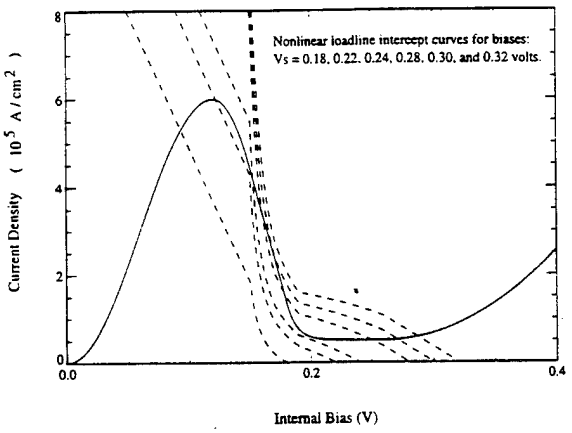

Fig. 11. Intersection curves of $I(V)$ characteristic and nonlinear loadline for a range of applied biases.

V_S-intercepts occur. Fig. 12 plots the overall current-density characteristic, for forward and backward bias sweeps, obtained from using the base circuit parameters $C_0 = 2.3 \times 10^{-7}$ F/cm^2 and $L_0 = 1.48 \times 10^{-21}$ H cm^2. In the forward sweep, oscillations are obtained in the voltage range (0.23. 0.30); however, these oscillations led to a very large downward shift in the average current. In the backward sweep, the circuit was stable over most of the hysteresis region with an up-shifting oscillation occurring over the voltage range $(0.23, 0.25)$. For both sweep directions the oscillations result from a process of cycling closely about a phase-space attractor point; hence, they are of a very high frequency (period $\ll 0.01$ ps) and small amplitude ($v \ll 0.01 \times 10^5$ A/cm^2). In addition, the average current results were found to be entirely independent of the values of L and C. This result differs greatly from a purely linear analysis [15] which predicts stable results if $RC < L|G|$. Since it is not possible to match either the forward-sweep plateau height or the nature of the oscillations observed in the physics-based simulations this model is an insufficient description of the RTD.

D. Parallel-Inductance Model: Nonlinear $R(V)$ Model

The transient response of the parallel-inductance model with nonlinear access resistance $R(V)$ and constant storage elements is described by the nonlinear equation

$$\frac{d^2v}{dt^2} + \eta(v, V_{\rm dc})\frac{dv}{dt} + \zeta(v, V_{\rm dc})\left(\frac{dv}{dt}\right)^2 + \omega^2(v, V_{\rm dc})v = 0 \quad (7)$$

where the coefficients are the same of those of (3) with R replaced by $R(V)$. Here, as in the last section, $V_{\rm dc}$ is found by solving the nonlinear loadline equation (i.e. see Fig. 12). The van der Pol algorithm was applied to this form of the parallel-inductance model to determine the phase-space trajectories. Fig. 13 displays the overall current-density results, for forward and backward sweeps, obtained from using the base circuit parameters $C_0 = 2.3 \times 10^{-7}$ F/cm^2 and $L_0 = 1.48 \times 10^{-21}$ H cm^2. These results indicate a very good match between the characteristic obtained from the circuit model and those of the physical simulations. For example, a forward-sweep plateau is present with correct magnitude (i.e. $\approx 4.5 \times 10^5$ A/cm^2) and extent (i.e. $V = 0.23$–0.30). Though not explicitly apparent in the *average* results of Fig. 13, the correspondence between the presence of oscillations and applied bias almost exactly matched the physical simulations in both the forward and backward sweep. Unfortunately, for the base inductor value L_0 the oscillations exhibited very large peak-to-peak swing and rapid jumps in the current-density at the phase-space turning points. However, when the inductor value was changed to $L = 5.5 \times 10^{-21}$ H cm^2 to tune the oscillation amplitude to the physics-based results at $V_S = 0.26$ V, a very good frequency-match was achieved over the entire plateau-region. For example, Fig. 14 gives the time evolution of the current-density at two different bias using this new value of L. As shown, the periods are now approximately 0.3 ps and 0.17 ps at $V_S = 0.26$ V and 0.28 V compared to quantum simulation results of 0.4 ps and 0.133 ps, respectively. While the dependance of oscillation amplitude on bias was not an exact match, these results identify the parallel-inductance circuit model, with nonlinear $R(V)$ element, as an excellent candidate for describing the dynamics of the RTD.

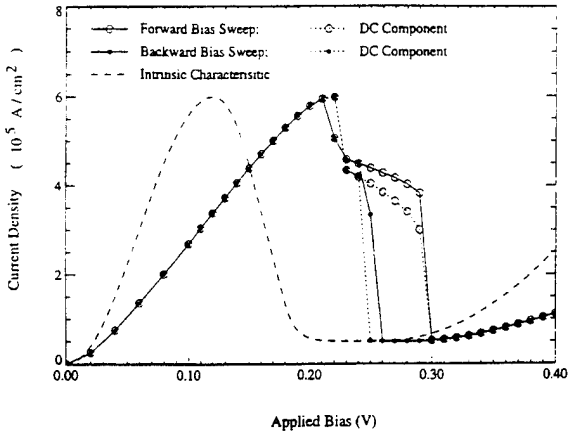

Fig. 13. Overall current-density versus applied bias derived from parallel-inductance circuit with nonlinear $R(V)$ model.

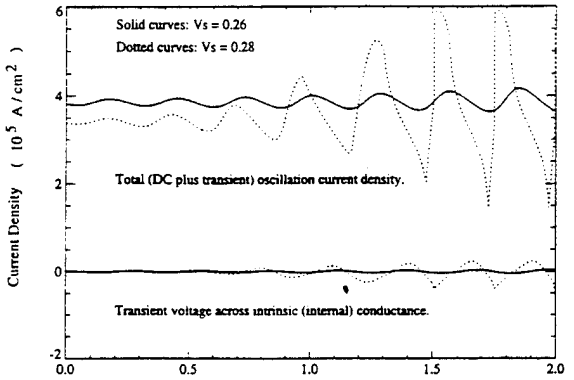

Fig. 14. Time evolution of the total current-density for the forward bias sweep at an applied bias of 0.26 and 0.28 V with $L = 5.5 \times 10^{-21}$ H cm^2. Here, the internal conductance biases (scaled by a factor of ten in volts) are also plotted for reference. Note, upper curves are current-densities and lower curves are internal bias.

E. Parallel-Inductance Model: Nonlinear $R(V)$ and $L(V)$ Models

The previous studies have shown that the parallel-inductance model with a nonlinear access can successfully match many of the characteristics associated with the self-oscillations of RTD's. The only real weakness of the model is its inability to simultaneously tune to the frequency and amplitude variations as a function of applied bias. Since the value of L directly modifies the growth/decay coefficients of the nonlinear transient equation given in (7), the introduction of a nonlinear inductance seems to be one possible approach of overcoming the limitations of the circuit model considered in the last section. In fact, Brown *et al.* [20] has previously proposed the introduction of a quantum well inductance given by $L_{QW} = \tau/G$ where τ is the quasibound state lifetime and G is the linear conductance, to describe the delay associated with resonant tunneling. Since this nonlinear study utilizes a nonlinear $I(V)$ characteristic, consistency requires the inductor model be of the form $\tau/G(V)$ which in our dc reference frame becomes $\tau/G(v, V_{dc})$. Note, when this model

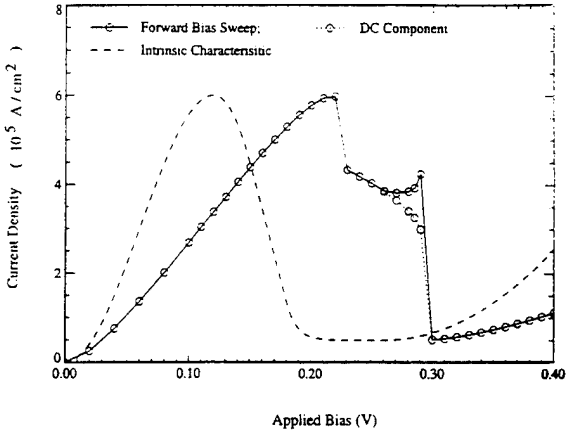

Fig. 15. Overall current-density versus applied bias derived from parallel-inductance circuit with nonlinear $R(V)$ model and nonlinear $L(V)$ model.

is utilized the inductor has a negative value for points inside the NDR region. With this inductance model, the dynamics are described by the nonlinear equation

$$\frac{d^2v}{dt^2} + \eta(v, V_{dc})\frac{dv}{dt} + \omega^2(v, V_{dc})v = 0 \qquad (8)$$

$$\eta(v, V_{dc}) = 1/\tau + 1/(R(v, V_{dc})C)$$

where

$$\omega^2(v, V_{dc}) = (R(v, V_{dc})g(v, V_{dc}) + 1)/(\tau R(v, V_{dc})C).$$

Notice that the introduction of this $L(V)$ model actually results in a simplified version of (7) where now the new coefficients in (8) are not able to become singular. The initial studies utilized the base circuit parameter $C_0 = 2.3 \times 10^{-7}$ F/cm^2 and the nonlinear access resistance $R(V)$ defined from Fig. 10. In addition, The initial value of τ was obtained by equating the nonlinear model for inductance, at the midpoint of the NDR region, to the base value of the inductance $L_0 = 1.48 \times 10^{-21}$ H cm^2. Utilizing this approach yields $\tau = L_0 G(V = 0.15\ \text{V}) = 0.015$ ps which is in approximate agreement which other estimations of tunneling time associated with the type of RTD under consideration [32]. Interestingly, this circuit model yielded results identical to the those obtained for the series-inductance circuit with a nonlinear $R(V)$ model studied in Section III-C. Hence, the introduction of Brown's inductance model removes the singularities that bound the oscillation to the NDR and allow the trajectory to converges to a phase-space attractor point. As in Section III-C, the overall current results of this circuit were found to be independent of L (i.e. τ) and C.

To gather additional information on the influence of nonlinear inductance on the parallel-inductance model, simulations were also performed for an inductance model defined from the *negative* of Brown's inductor model. Note, this results in a positive inductance inside the NDR region and a negative inductance outside the NDR region. For the initial studies utilizing the previous base parameters, trajectories for both the

forward and backward were found to become unbounded. To remedy this the state lifetime was increased to $\tau = 0.062$ ps (through a variational study) which yielded bounded limit cycles for the forward bias sweep. Fig. 15 shows the overall-current density for the parallel-inductance model with nonlinear access resistance and *negative* quantum-well inductance model. These results indicate that a nonlinear inductive effect can lift the higher-bias portion of the forward-sweep current-density plateau which is a characteristic observed in the physics-based results given in Fig. 2. The introduction of this horn in the $I(V)$ curve results from the nonlinear inductance which admits larger values of L for positive excursions about the $V_{\rm dc}$-intercept point. Unfortunately, in the unstable part of the backward bias sweep the oscillations were still found to become unbounded. Also, the amplitude of the forward-sweep oscillations still increases with increasing bias. However, the results of this section have shown that a nonlinear inductance element can be used to improve the match between the equivalent circuit model and the physics-based results.

IV. Conclusion

Numerically generated results have been used to judge the feasibility of a number of equivalent circuits presently in use to model the dynamics of resonant tunneling diodes (RTD's). In these studies two main circuit configurations were considered, each of which possesses the general electrical characteristics of RTD's. These studies have verified that neither configuration with constant R, L, and C elements is sufficient for describing the self-oscillations and overall current characteristics observed experimentally and predicted theoretically by fully self-consistent quantum mechanical simulations. These studies have shown that the introduction of nonlinear access resistance, with nonlocal dependence on the bias across the NDR current source (or equivalently the intrinsic double barrier structure), can improve the match to the hysteresis phenomena, in both circuit model configurations. However, only the circuit with a quantum-well inductance which directly chokes the nonlinear conductance element is capable of properly describing the current-plateau phenomena. In addition, this work has shown that incorporating nonlinearity effects into this inductive element can resolve some of the finer features of the oscillations and bistable behavior. While additional study is required to derive globally-accurate expressions for describing the full nonlinearity of the storage elements (i.e. L and C), this work has provided an improved tool for the optimization of RTD-based high frequency sources.

References

[1] L. L. Chang, L. Esaki, and R. Tsu, "Resonant tunneling in semiconductor double barriers," *Appl. Phys. Lett.*, vol. 24, pp. 592–595, June 1974.

[2] S. Luryi, "Frequency limit of double-barrier resonant-tunneling oscillators," *Appl. Phys. Lett.*, vol. 47, pp. 490–492, Sept. 1985.

[3] T. C. L. G. Sollner, W. D. Goodhue, P. E. Tannewald, C. D. Parker, and D. D. Peck, "Resonant tunneling through quantum wells at frequencies up to 2.5 THz," *Appl. Phys. Lett.*, vol. 43, pp. 588–590, Sept. 1983.

[4] E. R. Brown, J. R. Soderstrom, C. D. Parker, J. J. Mahoney, K. M. Molvar, and T. C. McGill, "Oscillations up to 712 THz in AlAs/AlSb resonant-tunneling diodes," *Appl. Phys. Lett.*, vol. 8, pp. 2291–2293, May 1991.

[5] E. R. Brown, "High-speed resonant-tunneling diodes," in *Heterostructures and Quantum Devices*, N. G. Einspruch and W. R. Frensley, Eds. Orland, FL: Academic, 1993, ch. 10, pp. 305–350.

[6] V. P. Kesan, D. P. Neikirk, P. A. Blakey, B. G. Streetman, and T. D. Linton, "The influence of transit-time effects on the optimum design and maximum oscillation frequency of quantum well oscillators," *IEEE Trans. Electron Devices*, vol. 35, no. 4, pp. 405–413, Apr. 1988.

[7] W. Liou and P. Roblin, "High frequency simulation of resonant tunneling diodes," *IEEE Trans. Electron Devices*, vol. 41, no. 7, pp. 1098–1111, July 1994.

[8] W. R. Frensley, "Quantum transport calculation of the small-signal response of a resonant tunneling diode," *Appl. Phys. Lett.*, vol. 51, no. 6, pp. 448–450, 1987.

[9] N. C. Kluksdahl, A. M. Kriman, D. K. Ferry, and C. Ringhofer, "Transient switching behavior of the resonant-tunneling diode," *IEEE Electron Device Lett.*, vol. 9, pp. 457–459, Sept. 1988.

[10] R. K. Mains and G. I. Haddad, "Wigner function modeling resonant tunneling diodes with high peak-to-valley ratios," *J. Appl. Phys.*, vol. 64, no. 10, pp. 5041–5044, 1988.

[11] C. Kidner, I. Mehdi, J. R. East, and G. I. Haddad, "Power and stability limitations of resonant tunneling diodes," *IEEE Trans. Electron Devices*, vol. 38, no. 7, pp. 864–872, July 1990.

[12] E. R. Brown, T. C. L. G. Sollner, C. D. Park, W. D. Goodhue, and C. L. Chen, "Oscillations up to 420 GHz in GaAs/AlAs resonant tunneling diodes," *Appl. Phys. Lett.*, vol. 55, no. 17, pp. 1777–1779, Aug. 1989.

[13] V. J. Goldsman, D. C. Tsui, and J. E. Cunningham, "Observation of intrinsic bistability in resonant-tunneling structures," *Phys. Rev. Lett.*, vol. 58, pp. 1256–1259, Mar. 1987.

[14] T. C. L. G. Sollner, "Comment on 'Observation of Intrinsic bistability in resonant—Tunneling structures," *Phys. Rev. Lett.*, vol. 59, pp. 1622–1623, Oct. 1987.

[15] F. A. Buot and K. L. Jensen, "Intrinsic high-frequency oscillations and equivalent circuit model in the negative differential resistance region of resonant tunneling diodes," *COMPEL*, vol. 10, no. 4, pp. 241–253, 1991.

[16] S. Yngvesson, *Microwave Semiconductor Devices*. Boston: Kluwer, 1991, ch. 4.

[17] P. Huang, "A microwave measurement technique for characterizing the I-V relationship for negative differential conductance devices," *IEEE Trans. Microwave Theory Tech.*, vol. 41, no. 8, pp. 1455–1458, Aug. 1993.

[18] R. J. Hwu, A. Djuandi, and S. C. Lee, "Negative differential resistance (NDR) frequency conversion with gain," *IEEE Trans. Microwave Theory Tech.*, vol. 41, no. 5, pp. 890–893, May 1993.

[19] O. Vanbesien, V. Sadaune, D. Lippens, B. Vinter, P. Bols, and J. Nagle, "Direct evidence of the quasibound-state lifetime effect in resonant tunneling from impedence measurements," *Microwave Opt. Technol. Lett.*, vol. 5, no. 8, pp. 351–354, Aug. 1992.

[20] E. R. Brown, C. D. Parker, and T. C. L. G. Sollner, "Effect of quasibound state lifetime on the oscillation power of resonant tunneling diodes," *Appl. Phys. Lett.*, vol. 54, no. 10, pp. 934–936, Mar. 1989.

[21] L. O. Chua, C. A. Desoer, and E. S. Kuh, *Linear and Nonlinear Circuits*. New York: McGraw-Hill, 1987.

[22] J. M. Gering, D. A. Crim, D. G. Morgan, P. D. Coleman, W. Kopp, and H. Morkoc, "A small-signal equivalent-circuit model for GaAs-$Al_xGa_{1-x}As$ resonant tunneling heterostructures at microwave frequencies," *J. Appl. Phys.*, vol. 61, no. 1, pp. 271–276, Jan. 1987.

[23] K. L. Jensen and F. A. Buot, "Numerical simulations of intrinsic bistability and high-frequency current oscillations in resonant tunneling structures," *Phys. Rev. Lett.*, vol. 66, no. 8, pp. 1078–1081, Feb. 1991.

[24] F. A. Buot and K. L. Jensen, "Lattice Weyl-wigner formulation of exact many-body quantum-transport theory and applications to novel solid-state quantum-based devices," *Phys. Rev. B*, vol. 42, pp. 9429–9457, 1990.

[25] F. A. Buot and A. K. Rajagopal, "High-frequency behavior of quantum-based devices: Equivalent-circuit, nonperturbative-response, and phase-space analyses," *Phys. Rev. B*, vol. 48, no. 23, pp. 17217–17232, 1993.

[26] B. van der Pol, "On 'Relaxation Oscillations," *Phil. Mag. Ser. 7*, vol. 2, pp. 978–992, 1926.

[27] E. R. Brown, W. D. Goodhue, and T. C. L. G. Sollner, "Fundamental oscillations up to 200 GHz in resonant tunneling diodes and new estimates of their maximum oscillation frequency from stationary-state tunneling theory," *J. Appl. Phys.*, vol. 64, no. 3, pp. 1519–1529, Aug. 1988.

[28] R. W. Horn, *Numerical Methods*. New York: Quantum, 1975.

[29] L. Brand, *Differential and Difference Equations*. New York: Wiley, 1966.

[30] C. Y. Belhadj, K. P. Martin, S. B. Amor, J. J. L. Rascol, R. C. Potter, H. Hier, and E. Hempfling, "Bias circuit effects on the current-voltage characteristics of double-barrier tunneling structures: Experiment and theoretical results," *Appl. Phys. Lett.*, vol. 57, no. 1, pp. 58–60, July 1990.

[31] H. C. Liu, "Simulation of extrinsic bistability of resonant tunneling structures," *Appl. Phys. Lett.*, vol. 53, no. 6, pp. 485–486, Aug. 1988.

[32] T. B. Bahder, C. A. Morrison and J. D. Bruno, "Resonant level lifetime in GaAs/AlGaAs double-barrier structures," *Appl. Phys. Lett.*, vol. 51, no. 14, pp. 1089–1090, Oct. 1987.

Dwight L. Woolard (S'91–M'92) was born in Washington, NC, on March 19, 1959. He received the Ph.D. degree in electrical engineering from North Carolina State University, Raleigh, in December 1991. Currently, he is a visiting research scientist with the Army Research Laboratory at Fort Monmouth, New Jersey, where his research is focused on the identification and physical modeling of electronic and optical devices for application to terahertz systems. His primary research interests include semiconductor device physics, quantum transport effects, modeling of electronic and optoelectronic devices, and numerical simulation techniques.

Felix A. Buot (M'84) received the Ph.D. degree in theoretical solid state physics from the University of Oregon, Eugene, and the M.S.E.E. degree from Stanford University, Stanford, CA.

He has held research positions at several institutions, including the University of London, the International Center for Theoretical Physics, McGill University, Stanford, and Cornell University. Since 1982, he has been at NRL as a research physicist and leads the efforts in nanoelectronics physics, modeling and simulation. He taught, part-time, a graduate physics course at George Mason University, Fairfax, VA. He has authored and co-authored more than 140 research publications and technical presentations. His research interests include interband and phase space dynamics of electrons in solids, mesoscopic physics and nanoelectronics, nonequilibrium quantum field theory, molecular electronic devices, fundamental physical limits of computation, performance and reliability analysis of novel high-speed heterojunction devices.

Dr. Buot is a member of the editorial board of *Transport Theory and Statistical Physics*, and has served in advisory committees, program committees, as session chairman, as convocation keynote speaker, and as an invited plenary speaker in several international conferences. He was a UNDP Consultant, National Institute of Physics, University of the Philippines, and University of San Carlos, summer of 1993. He is the recipient of several honors and awards; recently he won the 1990 and 1994 Alan Berman Research Publication Awards.

David L. Rhodes (S'80–M'80) received the B.S. degree in electrical engineering from Rutgers University, New Brunswick, NJ, in 1980 and the M.S. degree from Princeton University, Princeton, NJ, in 1982 while working at RCA Laboratories, David Sarnoff Research Center, Princton.

He joined RCA Laboratories in June 1980, working in the Microwave division. There he primarily worked on CAT and CAD for microwave applications including the areas of test automation, simulation, optimization, data visualization, and statistical design techniques. He is now Branch Chief of the Electrophysics and Modeling branch at the Physical Sciences Directorate (PSD) of the Army Research Laboratory (ARL), Fort Monmouth, NJ.

He is chair of the "IEEE SCC-30 MHDL Study Group" and is working on or directing efforts in the areas of parallel simulation, meta-modeling/statistical design, and active device modeling in addition to analog HDL-related work. He is currently tri-service leader of the Computational Electronics and Nanoelectronics area of High Performance Computing Modernization Program software initiative. He was the technical program chair for the first and second (1994 & 1995) "*International Conference on Electronic Hardware Description Languages (ICEHDL)*" (called SHDL in 1994) conferences. Mr. Rhodes is a member of the IEEE Circuits & Systems and Microwave Theory and Techniques societies and the Analog VHDL International's (AVI) Executive Committee. He also serves on the Editorial Board for the *International Journal of Microwave and Millimeter-Wave Computer-Aided Engineering*.

Xiaojia Lu received the B.S. degree in physics from Fudan University, Shanghai, China in 1982, the M.S. degree in electrical engineering from Shanghai Institute of Metallurgy, Shanghai, China, in 1985, and the Ph.D. degree in electrical engineering from Stevens Institute of Technology, Hoboken, NJ, in 1992.

After graduation, he worked as a postdoctorate at the University of Pittsburgh, where he worked on the design and fabrication of quantum well IR detectors. Since 1994 he has been working as a NRC research fellow at the U.S. Army Research Laboratory, Fort Monmouth, NJ. His current research interests include the design and fabrication of very high frequency circuitry and MMIC simulation and design.

Barry S. Perlman (M'65–SM'71–F'86) received the B.E.E. degree in electrical engineering from the College of the City University of New York in 1961, and the M.S.E.E. and Ph.D. degrees in electro-physics from the Polytechnic Institute of New York in 1964 and 1973, respectively.

He is currently Director, Electronics Division, U.S. Army Research Laboratory, Physical Sciences Directorate (ARL/PSD), Fort Monmouth, NJ. He is responsible for research and development of advanced electronic devices and technology to improve and enable new functionality in radar, EW, communications and smart weapons. He directs technical programs in high frequency electronics and monolithic circuits, millimeter-wave devices, quasioptics and photonics, electro-optical integration and prototyping, electrophysics and modeling, high speed/power devices, intelligent/neural electronics, signal processor prototyping, vacuum electronics, acousto-electronics and frequency control devices. Prior to his current position, he was Head, Design Research in the Microwave Laboratory at the David Sarnoff Research Center (formerly RCA Laboratories) in Princton, New Jersey.

Dr. Perlman is a member of Sigma Xi, a registered professional engineer in the State of New York and a member of IEEE Societies on Microwave Theory and Techniques, Circuits and Systems and Communications. He is a contributing member of the MTT AdCom where he serves as Chairman of the Intersocietal Liaison Committee and an active member of the Technical Program Committee. He serves as an Army representative to the Advisory Group on Electron Devices (AGED) and the DoD JDL/Reliance Sub Panel on Solid State RF Technology. He is a member of the Army's Electronic Coordinating Committee (ECOG), the Technical Advisory Committee (TAC) for the URI/High Frequency Microelectronics Center at the University of Michigan and the NSF/CAEME policy board at the University of Utah. He holds four U.S. patents and has published over 65 technical papers. He has received several awards including four RCA Outstanding Engineering Achievement Awards for research in microwave/millimeter-wave device and circuit technology.

ARMY RESEARCH LABORATORY
PHYSICAL SCIENCES DIRECTORATE
MANDATORY DISTRIBUTION LIST

Defense Technical Information Center*
ATTN: DTIC-OCC
8725 John J. Kingman Rd STE 0944
Fort Belvoir, VA 22060-6218
(*Note: Two DTIC copies will be sent from STINFO office, Ft. Monmouth, NJ)

Director
US Army Material Systems Analysis Actv
ATTN: DRXSY-MP
(1) Aberdeen Proving Ground, MD 21005

Commander, AMC
ATTN: AMCDE-SC
5001 Eisenhower Ave.
(1) Alexandria, VA 22333-0001

Director
Army Research Laboratory
ATTN: AMSRL-D (John W. Lyons)
2800 Powder Mill Road
(1) Adelphi, MD 20783-1197

Director
Army Research Laboratory
ATTN: AMSRL-DD (COL Thomas A. Dunn)
2800 Powder Mill Road
(1) Adelphi, MD 20783-1197

Director
Army Research Laboratory
2800 Powder Mill Road
Adelphi, MD 20783-1197
(1) AMSRL-OP-SD-TA (ARL Records Mgt)
(1) AMSRL-OP-SD-TL (ARL Tech Library)
(1) AMSRL-OP-SD-TP (ARL Tech Publ Br)

Directorate Executive
Army Research Laboratory
Physical Sciences Directorate
Fort Monmouth, NJ 07703-5601
(1) AMSRL-PS-A (V. Rosati)
(1) AMSRL-PS-T (M. Hayes)
(22) Originating Office

Advisory Group on Electron Devices
ATTN: Documents
Crystal Square 4
1745 Jefferson Davis Highway, Suite 500
(2) Arlington, VA 22202

Commander, CECOM
R&D Technical Library
Fort Monmouth, NJ 07703-5703
(1) AMSEL-IM-BM-I-L-R (Tech Library)
(3) AMSEL-IM-BM-I-L-R (STINFO Ofc)

ARMY RESEARCH LABORATORY
PHYSICAL SCIENCES DIRECTORATE
SUPPLEMENTAL DISTRIBUTION LIST
(ELECTIVE)

Deputy for Science & Technology
Office, Asst Sec Army (R&D)
(1) Washington, DC 20310

HQDA (DAMA-ARZ-D/
Dr. F.D. Verderame)
(1) Washington, DC 20310

Director
Naval Research Laboratory
ATTN: Code 2627
(1) Washington, DC 20375-5000

USAF Rome Laboratory
Technical Library, FL2810
ATTN: Documents Library
Corridor W, STE 262, RL/SUL
26 Electronics Parkway, Bldg. 106
Griffiss Air Force Base
(1) NY 13441-4514

Dir, ARL Battlefield
Environment Directorate
ATTN: AMSRL-BE
White Sands Missile Range
(1) NM 88002-5501

Dir, ARL Sensors, Signatures,
Signal & Information Processing
Directorate (S3I)
ATTN: AMSRL-SS
2800 Powder Mill Road
(1) Adelphi, MD 20783-1197

Dir, CECOM Night Vision/
Electronic Sensors Directorate
ATTN: AMSEL-RD-NV-D
(1) Fort Belvoir, VA 22060-5806

Dir, CECOM Intelligence and
Electronic Warfare Directorate
ATTN: AMSEL-RD-IEW-D
Vint Hill Farms Station
(1) Warrenton, VA 22186-5100

Cdr. Marine Corps Liaison Office
ATTN: AMSEL-LN-MC
(1) Fort Monmouth, NJ 07703-5033